Deep-level transient spectroscopy study of narrow SiGe quantum wells with high Ge content

K. Schmalz
Institute for Semiconductor Physics, Walter-Korsing-Strasse 2, 15230 Frankfurt (Oder), Germany

I. N. Yassievich
Ioffe Physico-Technical Institute, Polytechnicheskaya 26, 194021 St. Petersburg, Russia

E. J. Collart and D. J. Gravesteijn
Philips Research Laboratories, Prof. Holstlaan 4, 5656 AA Eindhoven, The Netherlands

(Received 16 July 1996)

We present a detailed theoretical and experimental study of hole emission processes in p-type Si/SiGe/Si structures under the nonequilibrium conditions found in deep-level transient spectroscopy (DLTS) investigations. We clarify the possibilities and limitations of DLTS applied to quantum-well (QW) structures. We report an observation of the effect of thermally activated tunneling induced by local high electric field on the emission rate of confined holes. In the limit of high external electric field F, the hole emission rate e_T increases with F according to $e_T = e_T(0)\exp(F^2/F_c^2)$, where the characteristic field F_c agrees with theoretical calculations. The effect of nonequilibrium carrier diffusion is determined from the dependence of the DLTS signal on the pulse frequency, allowing one to estimate the effective hole diffusion coefficient. Interface roughness scattering, which controls the carrier mobility in the narrow QW, is investigated. The observed diffusion coefficient depends only slightly on the width for the investigated narrow SiGe QW's (2–3 nm), but depends strongly on the Ge content ($x = 0.3$–0.5) in agreement with theory. A strong increase of the hole emission activation energy with decreasing nonequilibrium hole concentration gives evidence for considerable fluctuations of lateral potential, inducing lateral localization of confined holes at low temperatures. We show that interface roughness is responsible for these lateral potential fluctuations. [S0163-1829(96)08248-3]

I. INTRODUCTION

Space-charge spectroscopy techniques, such as admittance spectroscopy, deep-level transient spectroscopy (DLTS), and capacitance-voltage measurements (CV), are widely used for the characterization of quantum structure.[1,2] But, DLTS investigations of quantum-well (QW) structures can give rather contradictory results. For example, DLTS results of $A_{\rm III}B_{\rm V}$ semiconductor heterostructures[3–5] have not given clear evidence that a direct carrier emission from the QW was really observed. Such a conclusion could only be obtained when the carrier confinement in QW's was also investigated under equilibrium conditions by means of CV (Ref. 6) and admittance spectroscopy, revealing information on the carrier concentration in the QW and the potential barriers at the QW, respectively. The main problem for studying QW structures by DLTS is the lateral diffusion of confined carriers, leading to the situation that the carriers could be swept from the QW region beneath the Schottky contact laterally before hole emission across the barrier can occur.

This is the primary reason why in DLTS investigations of p-type Si/SiGe/Si QW's (Refs. 7–11) a strong DLTS signal is observed only in the case of mesa structures[8,9] or $Si_{1-x}Ge_x$ island layers.[10] Note that in contrast to the $A_{\rm III}B_{\rm V}$ semiconductor heterostructures a very small concentration of deep centers in the QW layer can be achieved for the state-of-the-art SiGe technology. This simplifies considerably the interpretation of DLTS data.

A rather broad band in the DLTS spectrum at lower temperatures, which was assumed to be due to a direct hole emission from the QW, was observed for structures with $x = 0.3$.[7] Theoretical and experimental results have been presented concerning the electrical characterization of p-type Si/SiGe/Si QW's by space-charge spectroscopy.[8,9] Hole emission from the QW region was observed by DLTS on n^+p mesa diodes for QW's with $x = 0.17$, but in the case of planar Schottky diodes for QW's with $x = 0.25$ no evidence was found for hole emission from the QW.[8] It was argued that in the case of planar Schottky diodes the holes could be swept from the QW region beneath the Schottky contact laterally before hole emission across the barrier can occur. A long enough hole storage time in the QW region, so that the hole emission becomes the dominating process, was realized for selectively grown $Si_{1-x}Ge_x$ layer with $x = 0.17$ and for a $Si_{1-x}Ge_x$ island layer with $x = 0.3$.[10] Direct hole emission was observed also for planar Schottky diodes on p-type $Si/Si_{1-x}Ge_x/Si$ with $x = 0.33$.[11] While the authors of Refs. 7 and 10 observed a DLTS peak for $x = 0.30$, that is broadened due to island distribution, the authors of Ref. 11 observed a narrow peak for a close concentration of $x = 0.33$. This should indicate that the QW layer in Ref. 11 is planar.

The aim of this paper is to present a detailed theoretical and experimental study of hole emission processes in p-type Si/SiGe/Si structures under the nonequilibrium conditions found in DLTS investigations, and to clarify the possibilities of DLTS applied to QW's.

We have investigated the role of carrier diffusion in the QW plane and the effect of local electric field on the formation of the DLTS signal. Good conditions for DLTS investigations of direct carrier emission from QW could be realized for (i) QW structures with low carrier mobility in the QW layer and/or (ii) QW structures with carrier localization beneath the contact region due to specially designed structures. Further, the possibility of thermally activated tunneling through the potential barrier due to the presence of a high electric field must be considered for the DLTS analysis.

A lower hole mobility was expected for narrow QW's with high Ge concentration, presumably because here alloy and roughness scattering decrease mobility, and therefore it should be easier to observe direct hole emission. To investigate the effect of lateral hole localization in the QW beneath the Schottky contact, we have used mesa Schottky diodes as well as planar Schottky diodes with various diameters. The effect of roughness scattering on carrier mobility in the QW is one of the dominating mechanisms for QW's.

Up to now, it has been assumed that scattering should decrease the mobility μ for narrow QW's according $\mu \sim d_{QW}^6$, where d_{QW} is the width of the QW. But, we show that this law is not valid for SiGe QW's, where the mobility only slightly depends on d_{QW} for d_{QW} in the region 2–4 nm according to our calculations.

Our experimental study combined CV, admittance, and DLTS investigations of narrow QW's with relatively high Ge content from $x=0.3$ to 0.5, to obtain reliable data for the electronic parameters of this QW structure. These include (i) the acceptor concentration, (ii) the concentration of confined holes in equilibrium and nonequilibrium conditions, (iii) the activation energy of the conductance across the QW, and (iv) the activation energy of hole emission rate from the QW as a function of the concentration of confined holes and the electric field.

The theoretical part of this paper deals with a detailed analysis of (i) thermally activated tunneling of confined holes enhanced by local high electric field, and (ii) the diffusion of nonequilibrium holes in narrow SiGe QW layers.

The paper is organized as follows. Section II describes the sample preparation. Section III gives experimental details and results of admittance and DLTS measurements. In Sec. IV we present the activation energies of thermal emission in equilibrium conditions, obtained by admittance spectroscopy for the QW's investigated. The activation energies are compared with theoretically calculated ones. In Sec. V we discuss the effect of thermally activated tunneling on the emission rate of confined holes and demonstrate how this effect can be deduced from the DLTS data. In Sec. VI we discuss the effect of lateral diffusion on the formation of the DLTS signal, and present experimental data on the lateral diffusion coefficient of confined holes. In Sec. VII we consider the effect of interface roughness scattering on hole mobility and the density of states of confined holes in narrow QW. Finally, Sec. VIII summarizes the most important conclusions.

II. SAMPLE PREPARATION

The p-type $Si/Si_{1-x}Ge_x/Si$ structures used in the present work were grown pseudomorphically in a modified solid source molecular-beam-epitaxy (MBE) system VG 80. The schematic picture of the structures used is given in Fig. 1. The epilayers were deposited onto (100) p^+-Si substrates, B doped, with a resistivity of 0.01–0.02 Ω cm. First, a 300-nm-thick buffer, B-doped to about 10^{17} cm^{-3} was grown at a substrate temperature of $T=630$ °C. For the individual structures, the $Si_{1-x}Ge_x$ layers with different thicknesses of 2 or 3 nm were sandwiched between 30-nm-thick undoped Si spacers. The SiGe layers were deposited at a substrate temperature of $T=630$ °C. Structures with $Si_{1-x}Ge_x$ layers with $x=0.3$, 0.4, and 0.5 were prepared. Finally, a 300-nm-thick B-doped Si cap layer with a dopant concentration of about 10^{17} cm^{-3} was deposited. The Ge sheet concentration of the SiGe was determined by Rutherford backscattering spectrometry (RBS). The Ge concentrations and the thicknesses of the SiGe layers for the investigated structures are given in Table I. The SiGe layer thickness was smaller than the critical value associated with strain relaxation by nucleation of misfit dislocations. We did not observe dislocation related peaks in the photoluminescence spectra of the investigated Si/SiGe/Si structures. The flatness of our Si/SiGe/Si structures as measured by means of Normarski interference microscopy is equal to that of MBE grown Si, and SiGe layers with x up to 0.5 were flat according to transmission electron microscopy. Further, our samples were grown extremely rapidly; i.e., 3 nm takes exactly 10 s to grow. Then the Ge shutter is closed and growth continues. So, no interruption takes place during growth, making the possibility of the formation of islands quite improbable.

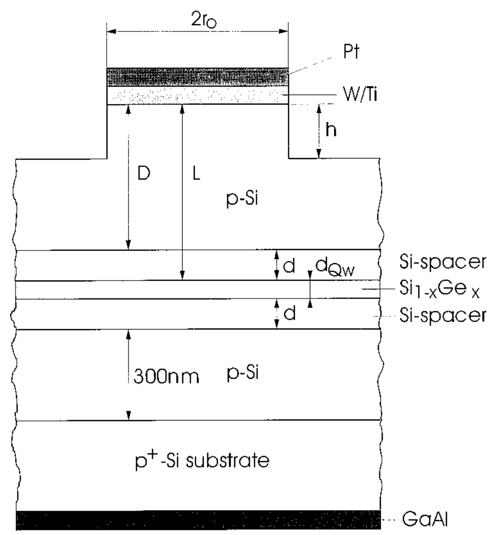

FIG. 1. Schematic picture of the mesa WTi Schottky diode used.

Schottky diodes were prepared by W/Ti deposition followed by Al or Pt deposition. The effective areas of the Schottky contact were $A=2.4\times10^{-3}$ cm^2 and 1.3×10^{-2} cm^2,

TABLE I. Ge concentration x and the thickness d_{QW} of the SiGe layer for the investigated structures.

Wafer	Thickness of SiGe layer (nm)	Ge sheet concentration x
T0309	2	0.3±0.02
T0312	3	0.3±0.02
T0310	2	0.4±0.02
T0307	3	0.4±0.02
T0304	2	0.5±0.04
T0308	3	0.5±0.025

respectively. For the CV and DLTS investigations we also used structures in which the thickness of the cap layer was reduced by chemically etching (surface layer removal up to 100 nm) to obtain an optimal thickness for these investigations. In order to obtain optimal conditions for DLTS measurements, we used a mesa Schottky diode geometry (Fig. 1) such that the $Si_{1-x}Ge_x$ layer did not penetrate the mesa, but formed a buried layer. We have not used structures ''mesa etched'' down to the QW layer in the present study, as for such structures (with open SiGe layer) we have observed unstable DLTS signals.

The DLTS measurements were performed with a commercial DLTS spectrometer (DLS-82 from SEMILAB, Hungary), and CV and admittance investigations were carried out using the impedance analyzer HP 4192A.

III. EXPERIMENTAL RESULTS

In this section we present experimental results on the concentration of confined holes and the hole thermal emission rate, obtained for narrow Si/SiGe/Si QW's at equilibrium and nonequilibrium conditions.

A. Capacitance voltage and admittance spectroscopy measurements

Here we present the results of capacitance voltage and admittance spectroscopy measurements, which give the concentration of confined holes and the activation energy of hole emission for equilibrium conditions. The condition, at which the QW becomes depleted, is found from the CV measurements.

The dependence of the capacitance C on the reverse bias U_R was obtained from the CV measurements performed at 1 MHz. The depth profile of the apparent carrier concentration $N=N(W)$ obtained from the dependence $C=C(U_R)$ is shown in Fig. 2 for a thinned sample. The $N(W)$ profiles for the samples give nearly constant acceptor concentrations N_{A1} and N_{A2} in the boron-doped cap and buffer layers above and below the SiGe layer, respectively. To obtain reliable data on N_{A2} the $C(U_R)$ measurements were also carried out on structures with a thinner cap layer. The values of the shallow acceptor concentrations N_{A1} and N_{A2} are given in Table II. For these samples a concentration peak appears in the $N(W)$ profile in the region of the QW, which is related to hole confinement in the QW.[2,8,12] The concentration n_w of confined holes was obtained from the $C=C(U_R)$ dependence for conditions, where the measurements at lower temperatures were not influenced by RC time constant effects.[2]

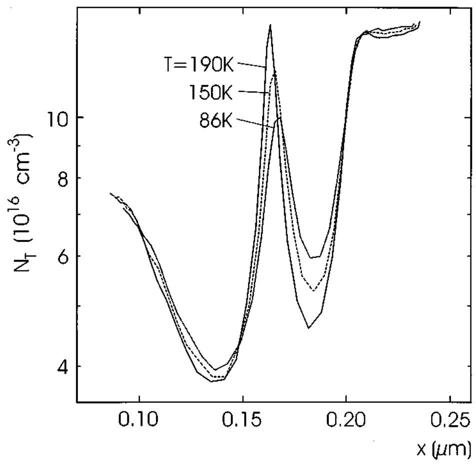

FIG. 2. Apparent carrier concentration profile $N=N(W)$ obtained from 1-MHz CV measurements at different temperatures (QW with Ge concentration $x=0.4$ and thickness $d_{QW}=2$ nm, thickness of the cap layer $D=200$ nm, height of the mesa $h=100$ nm).

The dependence C versus U_R (Fig. 3) for a structure with $x=0.5$ and $d_{QW}=2$ nm reveals a plateau of nearly constant capacitance C^*. The plateau between the first and second critical biases U_{R1} and U_{R2} is related to the hole concentration in the QW by $n_w=C^*(U_{R2}-U_{R1})/Ae$,[13] where A is the diode area and e is the elementary charge. Estimated n_w values for the used structures and the corresponding temperatures are given in Table II. Because the RC time constant effect in CV measurements at lower temperatures is related to the carrier confinement in the QW,[8] we were able to esti-

TABLE II. Experimental results of CV and admittance measurements.

Parameters of p-Si/$Si_{1-x}Ge_x$/Si d_{QW} (nm)	x	CV results N_{A1} (10^{17} cm^{-3})	N_{A2} (10^{17} cm^{-3})	n_w (10^{11} cm^{-2})	Admittance results E_a (meV)
2	0.3	0.8	1.2		51±1 (44–52 K)
3	0.3	0.4	0.9	1.6±0.2 (110 K)	94±3 (66–86 K)
2	0.4	0.8	1.3	1.7±0.2 (86 K)	83±2 (56–72 K)
3	0.4	0.7	1.1	2.0±0.2 (135 K)	113±3 (79–102 K)
2	0.5	0.8	1.5	2.7±0.2 (130 K)	125±3 (90–119 K)
3	0.5	0.5	0.9	3.1±0.2 (210 K)	166±3 (123–151 K)

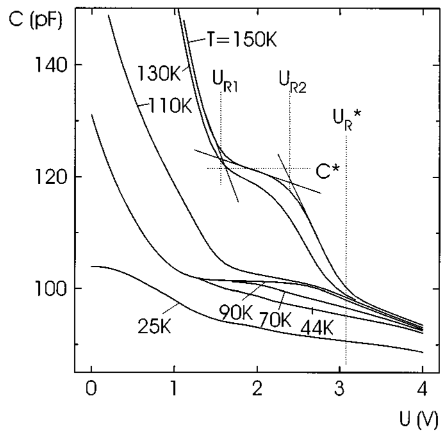

FIG. 3. Dependence of the capacitance C vs reverse bias U_R for 1-MHz measurements at different temperatures (QW with $x=0.5$, $d_{QW}=2$ nm, $D=250$ nm, $h=125$ nm, effective area of the Schottky contact $A=2.4\times10^{-3}$ cm^2): (a) 25 K, (b) 44 K, (c) 70 K, (d) 90 K, (e) 110 K, (f) 130 K, and (g) 150 K. The determination of the critical reverse biases U_{R1} and U_{R2} and of the capacitance value C^* is explained. The characteristic reverse bias U_R^* is also given.

mate the minimal reverse bias U_R^*, at which the QW becomes depleted, from the $C=C(U_R)$ relation measured at various temperatures.

Figure 3 shows two regions of reverse bias U_R, for which the dependence of $C(U_R)$ on the temperature is qualitatively different. In the region $U_R<U_R^*$ the capacitance $C(U_R)$ decreases strongly at lower temperatures due to RC time constant effects, but in the region $U_R\geqslant U_R^*$ the $C(U_R)$ curves do not depend strongly on the temperature. Thus, we can estimate U_R^* (Fig. 3).

For our Si/SiGe/Si structures with a 300-nm-thick cap layer and an acceptor concentration N_{A1} of about 10^{17} cm^{-3}, the SiGe layer is located in the neutral region at $U_R=0$. In this case, from the equivalent circuit for the space charge region of the Schottky diode with the QW in the neutral region, one obtains C_p and G_p (capacitance C and conductance G measured in a parallel equivalent circuit) as a function of C_1, C_2, G, and $\omega=2\pi f$, where C_1 is the capacitance of the space charge region of the Schottky diode, C_2 the capacitance of the QW, and G the conductance across the QW.[8,14] A maximum in $G_p(T)$ appears at $G^*=2\pi f(C_1+C_2)$. The temperature dependence of the conductance G of the QW is given by[8]

$$G(T)\sim T^{1/2}v_c\exp[-(eU_0+E_{\rm vb}-E_F)/k_BT],$$

where v_c is the QW capture velocity,[15] U_0 the potential barrier, $E_{\rm vb}$ the valence-band edge of the Si barrier, and E_F the Fermi level for holes. Hence, the resonance condition for the maximum in $G_p(T)$ determines the activation energy E_a, which can be obtained from the Arrhenius plot of $f/T^{1/2}$.

In Fig. 4 an Arrhenius plot of $f/T^{1/2}$ is presented for a structure with $x=0.3$ and $d_{QW}=2$ nm, giving an activation energy of $E_a=51$ meV. Figure 5 shows the $C_p(T)$ and $G_p(T)$ curves measured for structures with $d_{QW}=3$ nm and Ge concentration $x=0.3$, 0.4, and 0.5, respectively. The steplike change in $C_p(T)$ and the corresponding peak in $G_p(T)$ are shifted to higher temperatures for larger Ge concentration. The values of the activation energy E_a obtained from the Arrhenius plot of $f/T^{1/2}$ and the corresponding ranges of conductance peak temperatures are presented in Table II.

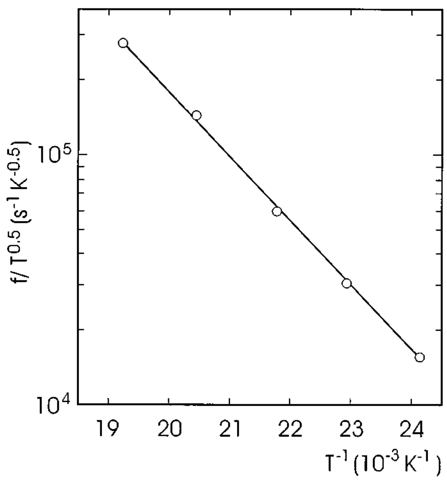

FIG. 4. Arrhenius plot of the normalized frequency $f/T^{1/2}$ of the conductance peak. The measurements were performed at $U_R=0.2$ V (QW with $x=0.3$ and $d_{QW}=2$ nm, $D=300$ nm).

B. DLTS measurements

Here we present the experimental results of DLTS measurements, which give the dependence of the activation energy of hole emission on the hole concentration and the electric field for nonequilibrium conditions.

We performed DLTS investigations at the minimum reverse bias U_R^*, at which the QW becomes depleted. This is the bias U_R^*, for which the electric field has only a minimal effect on the hole emission probability. For this condition, we performed DLTS measurements on the Si/SiGe/Si structures using planar Schottky diodes as well as mesa Schottky diodes (Figs. 6 and 7). A strong DLTS signal of peak amplitude $\Delta C/C$, related to hole emission from the QW, was ob-

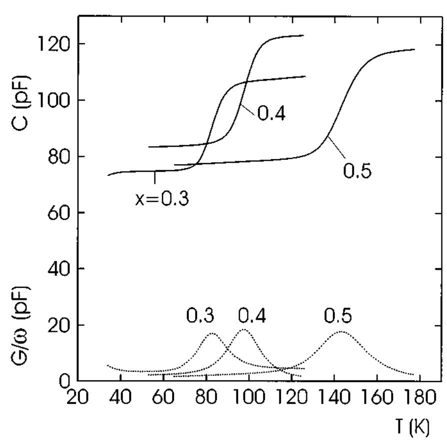

FIG. 5. Temperature dependence of the capacitance C (upper panel) and the normalized conductance G/ω (lower panel) for a measurement frequency $f=1$ MHz for 3-nm-thick QW's with different Ge concentration x: (a) 0.3, (b) 0.4, and (c) 0.5. ($D=300$ nm, $A=2.4\times10^{-3}$ cm^2, $U_R=0.2$ V).

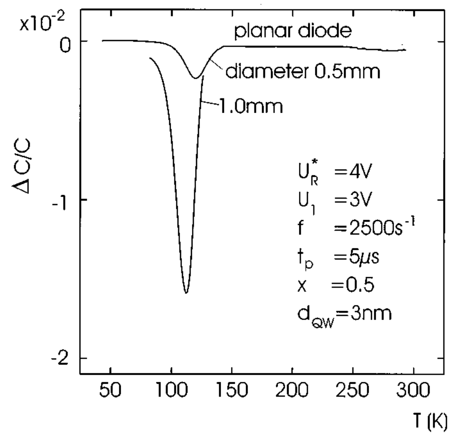

FIG. 6. Deep-level transient spectroscopy spectrum of a QW (Ge concentration $x=0.5$, QW thickness $d_{QW}=3$ nm) measured for various Schottky diode structures: (a) planar Schottky diode with diameter 0.5 mm and cap layer thickness $D=300$ nm, (b) planar Schottky diode with diameter 1 mm and $D=300$ nm, and (c) mesa Schottky diode with diameter 0.5 mm, mesa height $h=130$ nm and $D=240$ nm. The measurements were performed with pulse frequency $f=2500$ s^{-1} (corresponding to emission rate window $e_0=5580$ s^{-1}), pulse duration $t_p=5$ μs, reverse bias $U_R^*=4$ V and pulse bias $U_1=3$ V for (a) and (b), and $U_R^*=2.5$ V and $U_1=1.2$ V for (c), respectively.

served for the mesa Schottky diodes. For the mesa structure the lateral distribution of the surface potential can keep the holes beneath the Schottky contact for a longer time when switching the bias to the depletion mode. In the case of the planar Schottky diodes, the DLTS signal was much weaker, with the signal $\Delta C/C$ increasing with higher Ge concentration.

In planar Schottky diodes the lateral hole diffusion can decrease the hole concentration beneath the Schottky contact, and therefore causes a decreased DLTS signal. This is

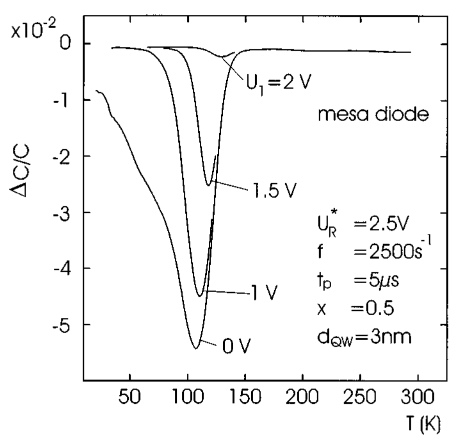

FIG. 7. Deep-level transient spectroscopy spectrum of a QW (Ge concentration $x=0.5$ and QW thickness $d_{QW}=3$ nm) measured for a mesa Schottky diode (diameter 0.5 mm, $h=130$ nm, $D=240$ nm) at the reverse bias $U_R^*=2.5$ V and the pulse frequency $f=2500$ s^{-1} (corresponding to emission rate window $e_0=5580$ s^{-1}) for different pulse biases U_1: (a) 0 V, (b) 1 V, (c) 1.5 V, and (d) 2.0 V. The pulse duration was $t_p=5$ μs.

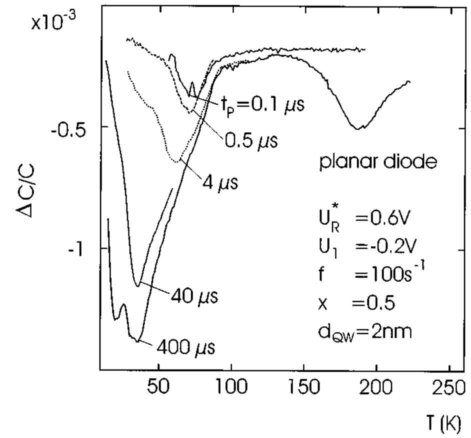

FIG. 8. Deep-level transient spectroscopy spectrum of a QW (Ge concentration $x=0.5$ and QW thickness $d_{QW}=2$ nm) measured for a planar Schottky diode (diameter 0.5 mm, cap layer thickness $D=210$ nm) at the reverse bias $U_R^*=0.6$ V, the pulse bias $U_1=-0.2$ V, and the pulse frequency $f=100$ s^{-1} (corresponding to emission rate window $e_0=220$ s^{-1}) for different pulse duration t_p: (a) 0.1 μs, (b) 0.5 μs, (c) 4 μs, (d) 40 μs, and (e) 400 μs.

supported by the following evidence. We prepared Schottky contacts with larger contact area (diameter varied in the range from 0.5 to 1.0 mm). These samples produced larger DLTS signals $\Delta C/C$. Figure 6 presents DLTS spectra of structures with $x=0.5$ and $d_{QW}=3$ nm, which were measured with the same DLTS parameters (pulse frequency f, reverse bias U_R, pulse bias U_1, pulse duration t_p) for planar Schottky diodes with diameters 0.5 and 1 mm. In order to determine the characteristic time of lateral hole diffusion, we also investigated the dependence of $\Delta C/C$ on the pulse frequency. The results are discussed in Sec. VI.

The DLTS peak shape was observed to depend strongly on the pulse bias U_1. For example, for larger pulse amplitude $(U_R^*-U_1)$ a broadening of the DLTS peak toward lower temperatures occurs. Figure 7 demonstrates this effect for a mesa Schottky structure with $x=0.5$ and $d_{QW}=3$ nm. However, this broadening, observed for a hole concentration in the QW larger than a certain critical concentration n_{wc}^*, depends also on the kind of structure under investigation. For example, the n_{wc}^* for the mesa Schottky diodes was considerably higher than for the planar Schottky diodes, and for planar Schottky diodes with a larger diameter. Therefore, this strong broadening of the DLTS peak seems not directly connected to hole emission across the potential barrier at the QW, or hole emission from defect states in the SiGe layer. More likely it is induced by a decay of nonequilibrium hole concentration n_w^* due to hole transport in the QW plane.

The dependence of the DLTS signal $\Delta C/C$ on the width t_p of the filling pulse showed that for larger n_w^* as in the case of the mesa structures, the maximum signal was obtained for a pulse width t_p of about 0.5 μs, indicating a fast hole capture. But, in the case of planar Schottky diodes, i.e., smaller values of n_w^*, the broadening of the DLTS spectrum was significantly stronger for longer t_p with $t_p \geqslant 5$ μs at lower pulse frequency f (Fig. 8). To avoid such influences on the analysis of hole emission from QW's, we have calculated the activation energy E_a of the hole emission rate e_T only from

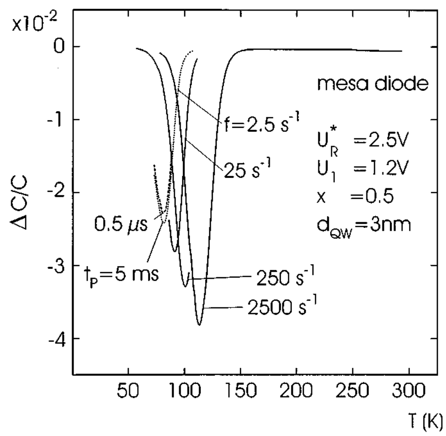

FIG. 9. Deep-level transient spectroscopy spectrum of a QW (Ge concentration $x=0.5$ and QW thickness $d_{QW}=3$ nm) measured for a mesa Schottky diode (diameter 0.5 mm, $h=130$ nm, $D=240$ nm) at the reverse bias $U_R^*=2.5$ V, the pulse bias $U_1=1.2$ V, the pulse duration $t_p=5$ μs, and for different pulse frequency f: (a) 2500 s^{-1}, (b) 250 s^{-1}, (c) 25 s^{-1}, as well as for $f=2.5$ s^{-1} with (d) $t_p=0.5$ μs and (e) $t_p=5$ ms.

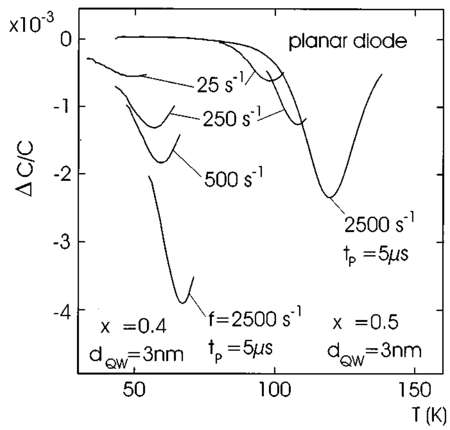

FIG. 10. Deep-level transient spectroscopy spectrum of QW structure: (a) Ge concentration $x=0.5$, QW thickness $d_{QW}=3$ nm, cap layer thickness $D=300$ nm, and (b) $x=0.4$ and $d_{QW}=3$ nm, $D=200$ nm, measured for a planar Schottky diode with diameter 0.5 mm. For (a) the reverse bias was $U_R=4$ V, the pulse bias $U_1=3$ V, the pulse duration $t_p=5$ μs, and the different pulse frequencies f (i) 25 s^{-1}, (ii) 250 s^{-1}, and (iii) 2500 s^{-1} were used. For (b) the parameters were $U_R=0.5$ V, $U_1=0.2$ V, $t_p=5$ μs, and f: (i) 25 s^{-1}, (ii) 250 s^{-1}, (iii) 500 s^{-1}, and (iv) 2500 s^{-1}.

DLTS measurements with $t_p=5$ μs. In the following, we focus only on such conditions for the pulse amplitude U_1, for which the broadening effect was not essential. DLTS spectra measured for such conditions at various pulse frequencies f, i.e., rate windows e_0, are depicted in Fig. 9 for a mesa structure, and in Fig. 10 for planar structures. It should be noted that the peak amplitude $\Delta C/C$ decreases with lower pulse frequency, particularly strong in the case of the planar Schottky structure.

The concentration n_w^* in the QW was estimated from $n_w^* = (\Delta C/C)(2N_A W^2/L)$,[3] with $\Delta C/C$ at $f=2500$ s^{-1} and taking for the acceptor concentration N_A the acceptor concentration N_{A2} in the buffer, i.e., $N_A=N_{A2}$. L is the thickness of the Si layer between the Schottky contact and SiGe layer, and W is the width of the depletion region. In the case of the mesa structures the maximal concentration n_w^* is of the same order of magnitude as the equilibrium hole concentration n_w, estimated from CV (Tables II and III).

According to Ref. 8, the thermal emission rate e_T of holes from the QW is given by

$$e_T=(2v_c/f\lambda_T)\exp[-(\Delta E_v-E_1)/k_BT],$$

where v_c is the QW capture velocity,[15] λ_T is the thermal length $\lambda_T=(2\pi\hbar^2/mk_BT)^{1/2}$ of holes with mass m, ΔE_v is the valence-band offset, and E_1 is the confinement energy of the first level. In the limit of narrow QW ($E_1 \gg k_BT$) the occupation factor f is one, and thus the preexponentional factor is proportional to $T^{1/2}$. This limit is fulfilled for our Si/SiGe/Si QW structures. We have calculated the activation energy E_a of hole emission from the Arrhenius plot of the normalized hole emission rate $e_T/T^{1/2}$ (Table III). Figure 11 shows the Arrhenius plots of the normalized hole emission rate $e_T/T^{1/2}$ for a QW with various nonequilibrium hole concentration n_w^*, which was realized by various pulse bias U_1. The activation energy increases for smaller concentration n_w^*.

The activation energy E_a, observed by DLTS for maximal hole concentration n_w^*, is in good agreement with the value of E_a, which was obtained by admittance spectroscopy (Tables II and III) giving evidence that the hole emission from the QW is really monitored by DLTS. But, for smaller hole concentration in the QW the activation energy increases significantly (Table III). This increase of E_a is larger for a higher Ge concentration.

The activation energy E_a is expected to decrease for higher electric fields, i.e., for larger reverse bias U_R. This dependence was investigated realizing the same hole concentration n_w^* for all U_R values by adjusting the same value of pulse bias U_1. On the other hand, according to $\Delta C/C = n_w^* L/(2N_A W^2)$ the dependence of the DLTS peak amplitude $\Delta C/C$ on the reverse bias U_R, which controls the depletion width W, allows one to also scrutinize the minimal reverse bias U_R^* at which the QW becomes depleted, determined from CV investigations. We remark that the DLTS peak amplitude and the peak temperature decrease for larger reverse bias. The slope of the Arrhenius plot of hole emission rate e_T decreases for larger U_R, as seen in Fig. 12 for structure with $x=0.5$ and $d_{QW}=3$ nm, where the parameter is $\Delta U_R=U_R-U_R^*$. The decrease of e_T as a function of the electric field F can be found from the dependence of $\ln[e_p(\Delta U_R)/e_p(0)]$ on ΔU_R at a given temperature (Figs. 12 and 13). A linear dependence was observed for the structure with $x=0.5$ and $d_{QW}=3$ nm (Fig. 13). For the structure with $x=0.5$ and $d_{QW}=2$ nm a transition from a linear to a quadratic dependence was detected (Fig. 14).

In this section we showed that the hole emission from the QW can be really studied by DLTS. This allows us to obtain the activation energy of the hole emission rate from the QW in dependence on the hole concentration for Si/SiGe/Si QW's with various Ge concentrations and SiGe layer thicknesses.

TABLE III. Experimental results of DLTS measurements.

QW	Admittance E_a (meV)	DLTS results E_a (meV)	DLTS results n_w^* (cm^{-2})
$x=0.3$			
$d_{QW}=2$ nm	51 ± 1 (44–52 K)		
$d_{QW}=3$ nm	94 ± 3 (66–86 K)	54 ± 3[a] (41–51 K)	7.2×10^9
		60 ± 3[a] (43–54 K)	5.1×10^9
		68 ± 2[a] (46–56 K)	3.0×10^9
		50 ± 3[b] (34–46 K)	4.1×10^9
		98 ± 3[b] (46–57 K)	9.6×10^8
$x=0.4$			
$d_{QW}=2$ nm	83 ± 2 (56–72 K)	39 ± 5[b] (37–46 K)	3.5×10^9
$d_{QW}=3$ nm	113 ± 3 (79–102 K)	94 ± 5[a] (52–67 K)	1.3×10^{10}
		103 ± 5[a] (55–69 K)	6.2×10^9
		119 ± 5[a] (59–74 K)	2.8×10^9
		118 ± 5[b] (60–74 K)	7.0×10^9
		171 ± 5[b] (73–83 K)	3.4×10^9
$x=0.5$			
$d_{QW}=2$ nm	125 ± 3 (90–119 K)	128 ± 5[a] (66–82 K)	7.5×10^{10}
		125 ± 5[a] (67–85 K)	5.1×10^{10}
		172 ± 5[a] (78–88 K)	1.7×10^{10}
		136 ± 5[b] (68–84 K)	4.4×10^9
$d_{QW}=3$ nm	166 ± 3 (123–151 K)	175 ± 5[a] (78–107 K)	1.4×10^{11}
		174 ± 5[a] (81–113 K)	9.9×10^{10}
		190 ± 5[a] (90–117 K)	6.5×10^{10}
		240 ± 5[a] (102–123 K)	2.3×10^{10}
		290 ± 5[a] (109–129 K)	5.7×10^9
		218 ± 5[b] (95–120 K)	7.5×10^9
		180 ± 5[c] (82–112 K)	4.5×10^{10}

[a]Mesa Schottky diode with diameter 0.5 mm.
[b]Planar Schottky diode with diameter 0.5 mm.
[c]Planar Schottky diode with diameter 1.0 mm.

IV. ACTIVATION ENERGY OF THERMAL EMISSION FOR EQUILIBRIUM CONDITIONS

In this section, we compare the experimental data on activation energies of the hole emission rate from Si/SiGe/Si QW's with theoretically calculated data.

The schematic valence-band profile for a p-type Si/SiGe/Si QW is given in Fig. 15. The QW's under study are so narrow that only three levels of space quantization occur for 2-nm QW thickness: heavy hole E_{1hh}, light hole E_{1lh}, and spin-orbit split hole E_{1so} and for 3-nm-thick QW additional second space quantization levels occur only for the heavy holes: E_{2hh}. Energy-level positions, band offsets, and masses for heavy, light, and spin-orbit split holes are presented for all investigated structures in Table IV. Here we have used the Luttinger parameters γ_1, γ_2, and γ_3 in dependence on the Ge content x, and the band offsets ΔE_{hh} ($\equiv\Delta E_v$), ΔE_{lh}, and ΔE_{so} according to Ref. 16. The effective masses for the Si barrier are also presented in Table IV ($x=0$).

In p-type $Si/Si_{1-x}Ge_x/Si$ QW structures the confined holes in the QW produce a depletion region in the vicinity of the QW due to charge neutrality. As a result, an electric potential barrier eU_0 appears and some shift of the bottom of the QW and energy-level positions is induced. For the narrow QW's under consideration only the first quantization level is populated, even at room temperature. The energy level E_{1hh} and the charge density of confined holes calculated by solving the Schrödinger's and Poisson's equations self-consistently[8] are presented in Table V.

For a 3-nm-thick QW with $x=0.5$, for example, the band offset is 398 meV, and the HH1 level is 84 meV from the bottom of the well for a populated well with two-dimensional concentration $n_w=8.8\times10^{11}$ cm^{-2}. In this case, the potential barrier relative to the Fermi level E_F in the barriers, i.e., $eU_0+E_{vb}-E_F$ (E_{vb}-valence-band edge in the barrier outside the space charge region[8]), is with $eU_0+E_{vb}-E_F=304$ meV much larger than the Fermi energy of confined holes $\varepsilon_F=10$ meV (relative to the HH1 level) and the thermal energy of 8 meV at 100 K. In Table V the results are also presented for the case of a smeared-out valence-band discontinuity with a characteristic length of intermixing $b=0.5$ and 1 nm, respectively; for details see Ref. 8.

Thus, the experimental values of the thermal activation

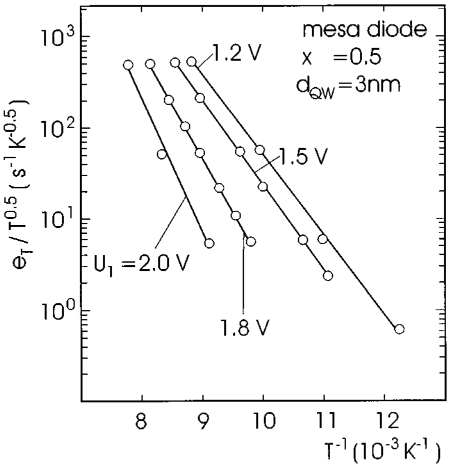

FIG. 11. Arrhenius plot of the hole emission rate e_T for QW with Ge concentration $x=0.5$ and QW thickness $d_{QW}=3$ nm, measured for a mesa Schottky diode (diameter 0.5 mm, $h=130$ nm, $D=240$ nm) at the characteristic reverse bias $U_R^*=2.5$ V. The parameter is the pulse bias U_1: (a) 1.2 V, (b) 1.5 V, (c) 1.8 V, and (d) 2.0 V, which corresponds to the following nonequilibrium hole concentration n_w^* (obtained from the DLTS peak $\Delta C/C$ at $f=2500$ s^{-1}): (a) 9.9×10^{10} cm^{-2}, (b) 6.5×10^{10} cm^{-2}, (c) 2.3×10^{10} cm^{-2}, and (d) 5.7×10^{9} cm^{-2}.

energy E_a, obtained from admittance spectroscopy (see Table II), are in good agreement with the theoretical values assuming a characteristic length of intermixing $b=1$ nm, but the confined hole concentrations n_w, estimated from the CV measurements, are smaller by about a factor of 2 than the theoretical concentration values. Note that interdiffusion at the Si/SiGe interface during MBE deposition determines the value of the intermixing parameter b, and therefore b is controlled by the substrate temperature during MBE deposition. It should be remarked that the roughness at the Si/SiGe in-

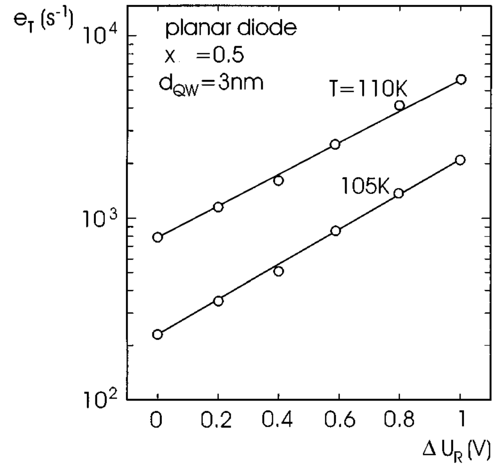

FIG. 13. Dependence of the hole emission rate e_T on the bias $\Delta U_R = U_R - U_R^*$ (U_R, reverse bias, characteristic bias $U_R^*=4$ V) obtained for QW (Ge concentration $x=0.5$ and QW thickness $d_{QW}=3$ nm) at (a) 105 K and (b) 110 K.

terface and fluctuations of SiGe alloy composition, which produces fluctuations of lateral potential, can also considerably shift the effective activation energy. It should be noted that the effect of the charge density of confined holes on the energy-level position E_{1hh} is very small for narrow QW's under consideration; see Tables IV and V.

V. THERMALLY ACTIVATED TUNNELING EFFECT FOR CONFINED HOLES

In this section we show that the observed dependence of the hole emission rate on the external electric field can be explained if thermally activated tunneling is taken into account.

The hole density n_w in the QW determines an electric

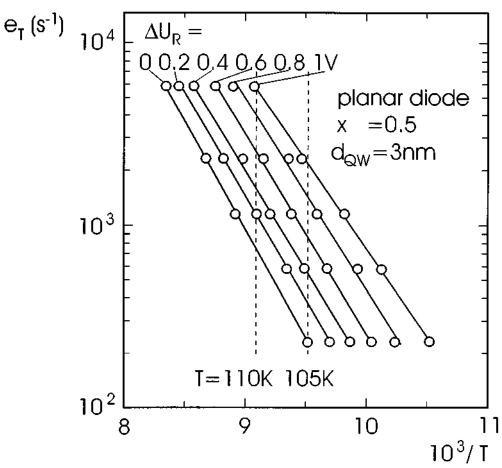

FIG. 12. Arrhenius plot of the hole emission rate e_T for QW's with Ge concentration $x=0.5$ and QW thickness $d_{QW}=3$ nm and cap layer thickness $D=300$ nm, measured for a planar Schottky diode with diameter 0.5 mm, obtained for different reverse bias U_R larger than the characteristic reverse bias $U_R^*=4$ V. Parameter is $\Delta U_R = U_R - U_R^*$: (a) 0 V, (b) 0.2 V, (c) 0.4 V, (d) 0.6 V, (e) 0.8 V, and (f) 1.0 V. The pulse bias U_1 was $U_1=3$ V.

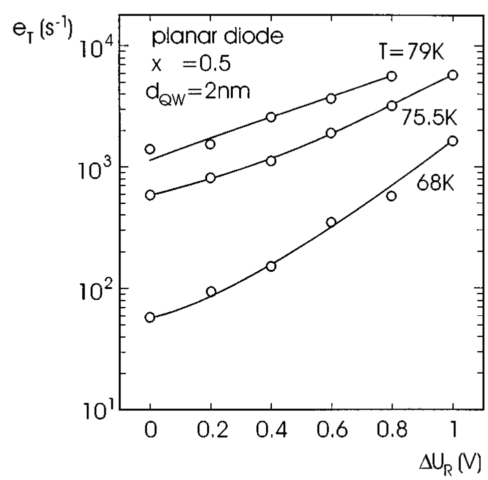

FIG. 14. Dependence of the hole emission rate e_T on the bias $\Delta U_R = U_R - U_R^*$ (U_R, reverse bias, characteristic bias $U_R^*=0.6$ V) obtained for QW (Ge concentration $x=0.5$ and QW thickness $d_{QW}=2$ nm) at (a) 68 K, (b) 75.5 K, and (c) 79 K. The measurements were performed at a planar Schottky diode with diameter 0.5 mm. The thickness of the cap layer was $D=210$ nm.

TABLE IV. Results of calculations for the confinement energy positions of heavy holes E_{hh}, light holes E_{lh}, and spin-orbit split holes E_{so}. The band offsets of heavy holes ΔE_{hh}, light holes ΔE_{lh}, and spin-orbit split holes ΔE_{so} as well as the masses m_{hh}, m_{lh}, and m_{so} are also given.

x	d_{QW} (nm)	m_{hh}	m_{lh}	m_{so}	ΔE_{hh} (meV)	ΔE_{lh} (meV)	ΔE_{so}	E_{hh}	E_{lh}	E_s
0		0.277	0.201	0.233						
0.3		0.260	0.167	0.203	0	−103	−169	(SiGe)		
					−238	−238	−282	(Si barrier)		
	2							−102	−193	−243
	3							−65	−170	−224
0.4		0.253	0.152	0.190	0	−138	−211	(SiGe)		
					−318	−318	−362	(Si barrier)		
	2							−119	−253	−304
	3							−74	−221	−278
								−259		
0.5		0.245	0.137	0.176	0	−172	−253	(SiGe)		
					−397	−397	−441	(Si barrier)		
	2							−135	−313	−365
								−393		
	3							−82	−272	−332
								−294		

field $F_0 = en_w/2\varepsilon_0\varepsilon_r$ at the boundaries of the QW, where $\epsilon_r\epsilon_0$ is the dielectric constant and e is the unit charge, e.g., $F_0 = 7.5\times10^4$ V/cm for $n_w = 2.5\times10^{11}$ cm^{-2}. In the case of DLTS measurements the reverse bias U_R applied to the Si/SiGe/Si structures increases the electric field in the vicinity of the QW, and further the DLTS measurements were performed at lower temperatures than in the case of admittance spectroscopy.

In a first step to describe quantitatively the thermally activated tunneling we calculated the electric field F in the vicinity of the QW as a function of the bias U_R applied to the structure, i.e., between the point $z=0$ (Schottky contact) and z_0 (the start of the neutral region below the QW) (Fig. 15). The following depletion regions are present: (1) in the cap layer of width D, i.e., $0 \leqslant z \leqslant D$; two regions of spacers (2) and (3), i.e., $D < z < D+d$ and $D+d \leqslant z < D+2d$; and (4) in the buffer below the QW, i.e., $D+2d \leqslant z \leqslant z_0$ (d thickness of the undoped spacer layers). We shall consider the QW with confined holes as a charge plane, i.e., $d_{QW}=0$, which gives a possibility to use the boundary conditions

$$[(\mathbf{F}_2 - \mathbf{F}_3)\mathbf{e}_z] = \frac{en_w}{\varepsilon_0\varepsilon_r},$$

where $\mathbf{e}_z$ is the unit vector normal to the QW plane, n_w is the hole density, and $\varepsilon_0\varepsilon_r$ is the dielectric constant in Si. F_2 and F_3 are the electric fields in spacers 2 and 3, respectively. The acting bias U_R, i.e., the applied bias plus the built-in potential of the Schottky contact, begins to decrease the concentration QW confined holes only, if

$$U_R \geqslant U_{R0}\left(1 - \frac{\eta}{4}\right), \qquad (1)$$

where

$$U_{R0} = \frac{eN_{A1}D^2}{2\varepsilon_0\varepsilon_r}, \quad \eta = \frac{2n_w^*}{N_{A1}D}. \qquad (2)$$

Here N_{A1} is the shallow acceptor concentration in the cap layer, and n_w^* is the actual concentration of confined holes for the DLTS measurement, which is usually less than the equilibrium concentration n_w in admittance measurements, and which can be controlled by the pulse bias U_1 of the DLTS measurement.

In this case, the electric field F_3 (in region 3), which determines the emission rate e_T of confined holes under reverse bias U_R, is found to be

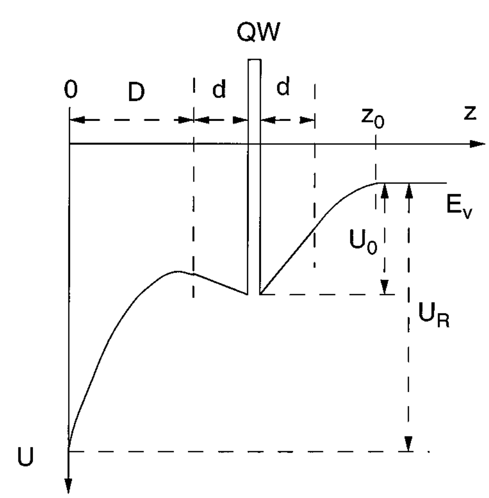

FIG. 15. Schematic valence-band profile for p-type Si/SiGe/Si QW at reverse bias U_R.

TABLE V. Results of self-consistent calculations for the confinement energy $E_{1\text{hh}}$, the Fermi energy E_F, the effective barrier $eU_0+E_{\text{vb}}-E_F$, and the two-dimensional hole concentration n_w. QW characteristics were also calculated assuming intermixing at the Si/SiGe interface with characteristic length b.

d_{QW} (nm)	d (nm)	x	b (nm)	$N_{A1}=N_{A2}$ (10^{17} cm^{-3})	T (K)	ΔE_{hh} (meV)	$E_{1\text{hh}}$ (meV)	$-E_F$ (meV)	$eU_0+E_{\text{vb}}-E_F$ (meV)	n_w (10^{11} cm^{-2})
2	30	0.3	0	1.5	45	239	103	25	133	3.5
				0			103			0
			0.5	1.5	45		140	25	98	2.3
			1.0	1.5	45		165		76	1.5
2	30	0.4	0	1.5	60	319	120	27	192	5.6
				0			119			0
			0.5	1.5	60		176	27	140	3.8
			1.0	1.5	60		214		105	2.5
2	30	0.5	0	1.5	90	398	134	32	255	7.5
				0			133			0
			0.5	1.5	90		211	32	184	5.2
			1.0	1.5	90		263		137	3.5
3	30	0.3	0	1.5	65	239	67	28	168	4.7
				0			66			0
			0.5	1.5	65		98	28	139	3.7
			1.0	1.5	65		134		106	2.5
3	30	0.4	0	1.5	80	319	76	30	235	6.9
				0			74			0
			0.5	1.5	80		120	30	194	5.6
			1.0	1.5	80		173		145	3.9
3	30	0.5	0	1.5	115	398	84	38	304	8.8
				0			81			0
			0.5	1.5	115		141	38	251	7.3
			1.0	1.5	115		210		187	5.1

$$F_3=\frac{2U_{R0}N_{A2}}{DN_{A1}}\times\left\{\sqrt{\left(1+\frac{2d}{D}\right)^2+\frac{N_{A1}}{N_{A2}}\left[\frac{U_R-U_{R0}}{U_{R0}}+\left(1+\frac{d}{D}\right)\eta\right]}-\left(1+\frac{2d}{D}\right)\right\}, \quad (3)$$

where N_{A2} is the shallow acceptor concentration in the buffer layer. Because for our structures $\eta<1$, we get from Eq. (3) in the case $\Delta U_R=U_R-U_{R0}<U_{R0}$,

$$F\approx\frac{\Delta U_R}{D(1+2d/D)}+\frac{U_{R0}(1+d/D)\eta}{D(1+2d/D)}. \quad (3')$$

We find $F_3\geqslant10^5$ V/cm for $\Delta U_R=2$ V, $D=200$ nm. Our estimation according to Ref. 17 has shown that an electric field of this order shifts the first energy level $E_{1\text{hh}}$ only few meV.

However, the thermally activated tunneling induced by the electric field F_3 in the vicinity of the QW can considerably decrease the effective activation energy. Taking into account the possibility of tunneling, we find that confined carriers thermally activated to an energy E less than the activation energy $E_a=(\Delta E_{\text{hh}}-E_{1\text{hh}})$ can be emitted.[8] In the important energy region of thermally activated tunneling only two or three levels of space quantization exist in our narrow QW's (Table IV). If the QW has ideal mirrorlike boundaries, and collisions during the time of tunneling can be neglected, the probability of tunneling is determined by the subband, to which the carriers belong. For a simple parabolic dispersion law this depends only on the position of the bottom of space quantization subbands, and is independent of the kinetic energy for motion along the QW. The effect of mixture of heavy, light, and spin-orbit holes, which takes place for complex valence bands, introduces the dependence of the tunneling probability on the lateral kinetic energy of confined holes. Besides, in our narrow QW the interface roughness produces fluctuations in the position of the space quantization levels. The same effect is induced by fluctuations of Ge content too. This gives us the possibility to disregard the discrete character of the spectrum and to suppose that the probability of tunneling depends only on the energy E, to which the hole is excited.

The probability of hole tunneling through a triangular barrier of height E_a-E in electric field F is proportional to $\exp[-4(E_a-E)^{3/2}(2m^*)^{1/2}/3\hbar eF]$, where m^* is the average effective mass for tunneling. The probability for it to be activated to level E is proportional to $\exp(-E/k_BT)$, where k_B is the Boltzmann constant. In this way, the emission probability of holes at energy level E is given by the product of a rising and a falling exponential function of E:

$$e_T(E,T,F) \sim \exp(-E/k_BT)\exp[-4(E_a-E)^{3/2} \times (2m^*)^{1/2}/3\hbar eF]. \quad (4)$$

The emission rate is determined by the optimal energy E_m at which the total exponent has a maximum:

$$E_m = E_a - \frac{1}{2m}\left(\frac{\hbar eF}{2k_BT}\right)^2. \quad (5)$$

Introducing E_m in Eq. (4) we get for the rate of thermally activated tunneling:

$$e_T = e_{T0}\exp(F^2/F_c^2), \quad (6)$$

where the characteristic electric field F_c is given by

$$F_c^2 = 24m^*(k_BT)^3/\hbar^2e^2, \quad (7)$$

and e_{T0} is the emission rate at $F=0$, $e_{T0} \propto \exp(-E_a/k_BT)$. For $m^*=0.2m_0$ (m_0 is the mass of the free electron), and $T=77$ K we get $F_c=4.5\times10^4$ V/cm. Therefore, we can expect according to Eqs. (6) and (3′) a strong dependence of the emission rate e_T on the applied reverse bias. For sufficiently large bias and low enough temperatures (in our case $T<100$ K) we have

$$\ln\left(\frac{e_T(F)}{e_{T0}}\right) = \frac{\Delta U_R^2}{D^2(1+2d/D)^2F_c^2}. \quad (8)$$

Figure 16 shows the experimental dependence of the emission rate on $(\Delta U_R)^2$ for the structures with $x=0.5$ and $d_{QW}=2$ nm. The theoretically expected dependence $\ln(e/e_0) \propto \Delta U_R^2$ is observed for $\Delta U_R \geqslant 0.4$ V. From the slope the value F_c can be determined using Eq. (8). We find $F_c=2.4\times10^4$ V/cm at $T=68$ K and $F_c=3.0\times10^4$ V/cm at $T=75$ K, which correspond to an effective mass of tunneling $m^*=0.1$. This value is reasonable as we deal with tunneling of confined holes belonging to light hole and/or spin-orbit split subbands. The relation between the F_c values for the two temperatures is 1.1; according to the theoretical law Eq. (7) 1.2 is expected. It should be noted that for small $\Delta U_R \leqslant 0.4$ V we observe a linear dependence $\ln(e/e_0) \propto \Delta U_R$, as well as for the sample with $x=0.5$ and $d_{QW}=3$ nm (see Fig. 13), for which a larger activation energy was measured (corresponding to higher temperature of measurements). Such linear dependence according to Eqs. (3′) and (6) should be observed if $\Delta U_R \leqslant U_{R0}\eta$ and the constant term in Eq. (3′) should be taken into account. Note that the characteristic electric field F_c decreases strongly with temperature; see Eq. (7). In the case of structures with smaller activation energy E_a, e.g., for $x=0.3$ and 0.4, E_a was measured by DLTS in a temperature region (see Table III) where the internal electric field $F_0=en_w^*/2\varepsilon_0\varepsilon_r$, induced by nonequilibrium confined holes, was itself larger than F_c, and therefore thermally activated tunneling decreases the activation energy already at the minimal bias U_R^*. Thus, it is not a surprise that the E_a values measured by DLTS are smaller for these structures than the ones that were obtained by admittance measurements, where the measurements were carried out at considerably higher temperatures.

In this section we calculated the electric field in the vicinity of the SiGe layer as a function of the reverse bias applied to the Si/SiGe/Si structure. This allows us to analyze the experimental dependence of the hole emission rate on the reverse bias, and to verify thermally activated tunneling of holes in strong electric field.

VI. LATERAL HOLE DIFFUSION EFFECT

In this section we analyze the role of lateral hole diffusion on the formation of the DLTS signal. A DLTS signal due to hole emission from a QW can be observed only if substantial hole diffusion in the QW plane is suppressed.[8] In the present work we have realized such suppression by a mesa Schottky diode structure due to the surface potential around the mesa, which leads to potential barriers for the lateral hole transport. In this case, the maximal nonequilibrium hole concentration n_w^*, estimated from the DLTS signal $\Delta C/C$, was only a few times smaller than the equilibrium concentration n_w obtained by admittance spectroscopy measurements (Tables II and III). However, for the planar Schottky diodes a considerably smaller concentration n_w^* was obtained (Table III). The nonequilibrium concentrations n_w^* were found to decrease strongly for lower filling pulse frequency f; see Fig. 10. Characteristic dependences of n_w^* on the reverse frequency $1/f$ are presented in Fig. 17.

To analyze the dependence of the concentration n_w^* on the frequency f, we shall consider the decay in the average hole concentration under the Schottky contact due to hole diffusion during the time interval between two filling pulses. Under equilibrium conditions the concentration of confined holes in the QW plane is uniform and equal to n_{w0}. If at moment $t=0$ the reverse bias U_{R1} is applied to the Schottky contact, the holes in the region under contact undergo a potential change ΔU_{R1}, and therefore the holes can be swept from the QW region beneath the Schottky contact laterally before hole emission across the barrier can occur. Thus, for $e\Delta U_{R1} > k_BT$, we arrive at a diffusion problem in the region $0<r\leqslant r_0$, where r_0 is the radius of the Schottky contact, with the initial condition $n_w=n_{w0}$ at $t=0$ and the boundary condition $n_w(r_0,t)=0$. The solution of this problem for the average concentration under the contact

$$\langle n_w(t)\rangle = \frac{2}{r_0^2}\int_0^{r_0} n(r,t)r\ dr \quad (9)$$

gives

$$\frac{\langle n_w(t)\rangle}{n_{w0}} = \sum_{m=1}^{\infty}\frac{4}{\alpha_m^2}\exp\left(-\frac{\alpha_m^2D_ht}{r_0^2}\right), \quad (9')$$

where D_h is the diffusion coefficient of two-dimensional holes, and α_m is the mth root of the Bessel function of zero order $J_0(z)$: $\alpha_1=2.41$, $\alpha_2=5.52$. If we take into account only the main first term in Eq. (9′) we get

$$\langle n_w(t)\rangle/n_{w0} = 0.69\ \exp(-5.8D_ht/r_0^2). \quad (9'')$$

According to Eq. (9″) the concentration n_w^* is plotted in Fig. 17 as a function of $t=1/f$ (f is the pulse frequency) for the structures with $x=0.5$ and $d_{QW}=3$ nm and 2 nm, respectively. Only the initial region of this dependence gives approximately an exponential decay $n_w^*(t)=n_w^*(0)\exp(-t/t^*)$

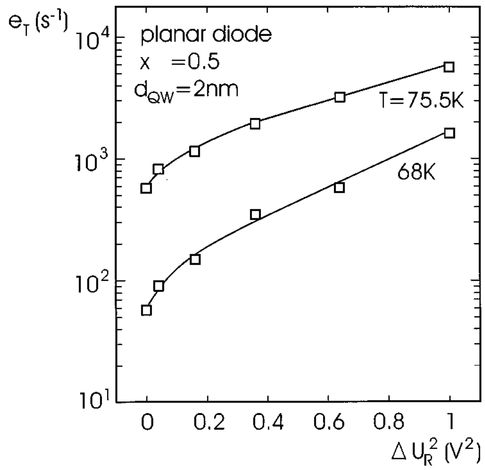

FIG. 16. Dependence of the hole emission rate e_T on the bias $\Delta U_R = U_R - U_R^*$ (U_R, reverse bias, characteristic bias $U_R^* = 0.6$ V) obtained for QW (Ge concentration $x=0.5$ and QW thickness $d_{QW}=2$ nm) at (a) 68 K and (b) 75.5 K, plotted as e_T vs $(\Delta U_R)^2$.

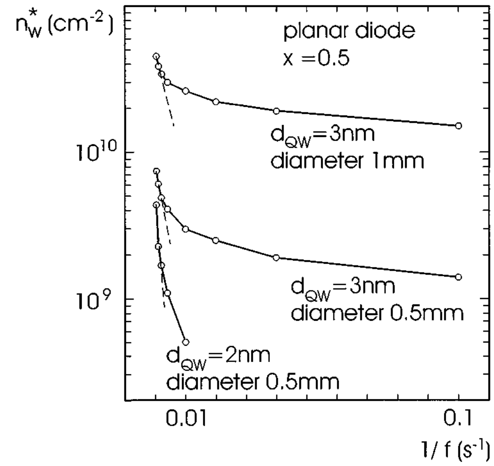

FIG. 17. Dependence of the hole concentration n_w^* on the reverse pulse frequency $1/f$ obtained for planar Schottky diode on a structure with Ge concentration $x=0.5$, QW thickness $d_{QW}=3$ nm, and cap layer thickness $D=300$ nm: (a) diameter 1 mm, (b) diameter 0.5 mm, and (c) on a structure with $x=0.5$, $d_{QW}=2$ nm, and $D=210$ nm for a planar Schottky diode with diameter 0.5 mm.

with characteristic time t^*. We argue that this is due to a strong decrease of the diffusion coefficient D_h with decreasing hole concentration. Therefore, a characteristic time t^* was only obtained from the initial slope. From this t^* an effective diffusion coefficient $D_h = 0.02$ cm^2/s was estimated for the structures with $x=0.5$ and $d_{QW}=3$ nm in the case of planar Schottky diodes with diameter 0.5 mm. $D_h = 0.01$ cm^2/s was found for the structure with $x=0.5$ and $d_{QW}=2$ nm. Such small values of the effective diffusion coefficient should be connected with the presence of great fluctuations of lateral potential in QW's under consideration, as discussed in the next paragraph.

To substantiate the role of lateral diffusion in the formation of the DLTS signal we have prepared Schottky diodes with various diameters. The concentration n_w^* increases with larger diameter (Table III). However, the characteristic time t^* does not change as strongly as expected from Eq. (9″). We estimated from the initial slope $t^* = 5\times10^{-3}$ s^{-1} for structures with $x=0.5$ and $d_{QW}=3$ nm and diameter 0.5 mm, and $t^* = 6\times10^{-3}$ s^{-1} for diameter 1 mm. We argue that this is due to a strong dependence of the diffusion coefficient D_h on the hole concentration, which is also not uniform under the Schottky contact. Such a strong decrease of D_h with lower hole concentration could also explain the discrepancy between the experimentally found dependence of n_w^* and the expected single exponential decay.

VII. INTERFACE ROUGHNESS SCATTERING EFFECT

In this section we analyze the role of interface roughness scattering in lateral mobility of holes confined in narrow Si/SiGe/Si QW's, and demonstrate that the experimental results on lateral diffusion are in qualitative agreement with theoretical considerations.

The interface roughness scattering is usually considered as dominating for narrow QW's because the mobility μ limited by interface roughness was assumed to decrease with QW thickness d_{QW} according to the law $\mu \sim d_{QW}^6$ (Refs. 18–21). For example, the theoretical calculations[18] of mobility limited by interface roughness scattering for SiGe QW with $x=0.4$ and amplitude of roughness $\Delta = 0.5$ nm have given a mobility $\mu = 200$ cm^2/V s for QW of thickness 3 nm, and correspondingly μ should be one order smaller for 2 nm. Experimentally we did not find a great difference in the diffusivity, being related to mobility, between the investigated structures with thicknesses 2 and 3 nm, for example, for Ge content $x=0.5$.

The law $\mu \sim d_{QW}^6$ was observed experimentally in GaAs QW layers[21] for the electron mobility in selectively doped n-Al$_x$Ga$_{1-x}$As-AlAs-GaAs-AlAs structures, with varying thicknesses from 4 to 7 nm. In Ref. 21 the characteristic parameters, i.e., the height of roughness Δ and correlation length Λ, which are usually introduced to describe the interface roughness scattering, the values $\Delta = 0.28$ nm and $\Lambda = 5$–7 nm were obtained by fitting the mobility dependence on the QW thickness. Note that for this structure the band offset between GaAs and AlAs is 1.2 eV, and therefore the theoretical approximation of infinitely large barriers, which was used to obtain the law $\mu \sim d_{QW}^6$, is valid.

However, for narrow QW's in the general case this law should be modified. Actually, there are two limiting analytical expressions for the lowest space quantization level: (i) the infinite-barrier model

$$E_1 = \frac{\hbar^2}{2m_w}\left(\frac{\pi}{d_{QW}}\right)^2; \tag{10}$$

(ii) for ultrathin QW,

$$E_1 = \Delta E_v - \frac{m_w^2 d_{QW}^2}{m_b 2\hbar^2}(\Delta E_v)^2, \tag{11}$$

where m_w and m_b are effective masses (in the direction perpendicular to the QW plane) in the QW and barrier layers, respectively, and ΔE_v is the band offset.

Equation (10) can be only applied if the QW power w is much larger than unity, w is defined as

$$W=\sqrt{\frac{2m_w\Delta E_v d_{QW}^2}{\hbar^2}}. \quad (12)$$

The opposite limiting case corresponding to Eq. (11) occurs if $w\ll 1$. Note that in experiments of Ref. 21 $3.5\leq w\leq 6.1$, but in our experiments $1.5\leq w\leq 2.9$.

To describe the interface roughness scattering, the scattering potential $\delta V(r)$ is introduced by

$$\delta V(\mathbf{r})=\frac{\partial E_1}{\partial d_{QW}}\Delta(\mathbf{r}), \quad (13)$$

where $\Delta(\mathbf{r})$ is a random modulation of the QW width d_{QW}, which changes the position of the subband levels, $\mathbf{r}$ is a vector in the plane of the QW. Here only the first subband E_1 ($E_1\equiv E_{1hh}$) is under consideration. The roughness is characterized by two parameters: the average height Δ and the correlation length Λ. For a Gaussian distribution function of the roughness we have

$$\langle\Delta(\mathbf{r})\Delta(\mathbf{r}')\rangle=\Delta^2\exp\left[-\left(\frac{\mathbf{r}-\mathbf{r}'}{\Lambda}\right)^2\right]. \quad (14)$$

This approach is only justified if Δ is much smaller than the QW width. The law $\mu\sim d_{QW}^6$ was obtained from Eqs. (10) and (13), that is, in the limit $w\gg 1$, and assuming an average scattering matrix element, which determines the relaxation momentum time, i.e., mobility, is proportional to $(\partial E_1/\partial d_{QW})^{-2}$.

In Fig. 18 the calculated value for $(\partial E_1/\partial d_{QW})$ is presented as a function of the QW width d_{QW} for different Ge concentrations x, e.g., $x=0.3$, 0.4, and 0.5, as well as for the two limiting approximations. Since the mobility should be proportional to $(\partial E_1/\partial d_{QW})^{-2}$ we find that the decrease of mobility from $d_{QW}=3$ to 2 nm is only about a factor of 2 for all considered Ge concentrations. A similar reduction in mobility is expected by changing Ge content from $x=0.3$ to 0.5. We suppose that our data demonstrate the importance of interface roughness scattering for QW's under study.

As a next step we will determine the change in density of states of confined holes due to interface roughness. The single-particle relaxation time of holes with kinetic energy ε,[22] which determines the density of states of disordered confined holes in the lowest order of roughness-hole interaction, is given by

$$\frac{1}{\tau(\varepsilon)}=\sqrt{\frac{\pi m}{2\varepsilon}}\frac{\Delta^2\Lambda}{\hbar^2}\left(\frac{\partial E_{1h}}{\partial d_{QW}}\right)^2, \quad (15)$$

where m is the effective mass for lateral motion at kinetic energy ε. Note that in the case of momentum relaxation time,[22] which determines the conductivity, Eq. (14) should contain an additional factor $\hbar^2/2m\varepsilon\Lambda^2$.

In order to obtain Eq. (15) we have neglected the screening effect produced by confined holes. The energy $\hbar/\tau(\varepsilon_F)$ (calculated at Fermi energy $\varepsilon=\varepsilon_F$) gives an estimate of the fluctuation amplitudes of occasional lateral potential. Of course, this estimate is very rough, because the electron-electron interaction, which is very important for a disordered two-dimensional carrier gas,[23,24] is not taken into account. From Eq. (15) we obtain for $d_{QW}=2$ nm and $x=0.5$ at $\varepsilon_F=10$ meV a value $\hbar/\tau(\varepsilon_F)\approx 100$ meV, if we assume $\Delta=0.28$ nm and $\Lambda=7$ nm as in Ref. 21. The same estimate performed for structures with $x=0.3$ and $d_{QW}=3$ nm gives an occasional potential of about 20 meV.

Actually, in our experiments the activation energy E_a increases for lower concentration n_w of confined holes (Table III), where the larger deviation ΔE_a was observed for higher Ge concentration. The value of ΔE_a is in reasonable agreement with the estimated energy $\hbar/\tau(\varepsilon_F)$. Thus, at low temperatures we deal with confined holes located in occasional potential wells induced by roughness, because $\hbar/\tau(\varepsilon_F)>\varepsilon_F$. Thus, only a small part of confined holes, which have an energy above the percolation level ε_c, can take part in lateral transport.[25,26] For estimation, we assume ε_c to be about 0.5 of the amplitude of occasional potential, e.g., for our structures ε_c is in the range from 10 to 50 meV. In this case the effective diffusion coefficient is low and has a thermally activated temperature dependence

$$D_h=D_{0h}\exp[-(\varepsilon_c-\varepsilon_F)/k_BT]. \quad (16)$$

The percolation level ε_c, i.e., the ''mobility edge,'' separates nonlocalized states from the tail of localized states, where the density of states $\rho(\varepsilon)$ decreases with smaller energy $\varepsilon(\varepsilon<\varepsilon_c)$ according to the law

$$\rho(\varepsilon)=\rho(\varepsilon_c)\exp\left[-\left(\frac{\varepsilon_c-\varepsilon}{\varepsilon_c}\right)^v\right], \quad (17)$$

where the index v is of the order of unity for almost all theoretical models.[25]

Therefore, a strong dependence of the effective activation energy E_a measured by DLTS as well as one of the mobility of confined holes on the concentration n_w^* should be found, because the upper energy level populated by nonequilibrium holes is determined by n_w^*.

Further, the appearance of small activation energies of a few tens of meV in the DLTS spectra, suggested by the strong DLTS signal at low temperatures (of about 30 K; see Figs. 7 and 8), could be related to a thermally activated hole diffusion out of the Schottky contact region. At these temperatures the characteristic rate of the hole diffusion process is assumed to be in the range of the emission rate window for the DLTS measurement. In this case, a strong dependence of the diffusion coefficient on the confined hole concentration n_w could explain the observed broad DLTS spectra; see Fig. 7.

In all samples, the deviation ΔE_a is in reasonable agreement with theoretical estimation. However, the largest deviation has been observed for structures with $x=0.5$ and $d_{QW}=3$ nm, but theory predicts the largest value for structures with $x=0.5$ and $d_{QW}=2$ nm. Maybe this fact is connected with the appearance of Ge clusters.

We have also calculated the input of alloy scattering in the mobility for samples under investigation by using the same approach that has been applied in the case of interface roughness scattering. The results show that alloy scattering may be important only if clusters of Ge atoms appear. Note that a strong decrease of mobility due to clusters was observed in a bulk SiGe alloy with small Si content.[27]

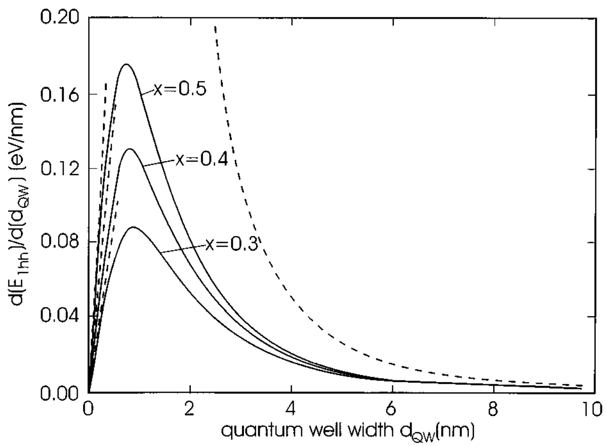

FIG. 18. The calculated value $\partial E_1/\partial d_{QW}$ vs the thickness d_{QW} of the QW for Ge concentrations $x=0.3$, 0.4, and 0.5. The curves for the limit approximations of (a) the infinite-barrier model and (b) the ultrathin QW are also given.

VIII. CONCLUSIONS

Thermally activated tunneling and lateral diffusion of confined holes play an important role in the formation of the DLTS signal for QW structures. We have observed thermally activated tunneling, which depends on the applied external electric field. This allows one to estimate the effective mass (for tunneling) of highly excited holes. The activation energies of hole emission, determined by admittance spectroscopy for equilibrium conditions, and measured by DLTS under low electric field and for higher nonequilibrium hole concentrations are in good agreement. This indicates that in this case, the influence of the local electric field is not essential, and therefore the activation energy can be used for the determination of the band offset.

The observed strong increase of the activation energy with decreased nonequilibrium hole concentration can yield an estimate of the amplitude of lateral potential fluctuations.

We have taken into account interface roughness scattering for analyzing the dependence of the DLTS signal amplitude on the pulse frequency. The magnitude of this scattering depends only slightly on the width of the QW for the investigated QW's with width 2–3 nm, but increases with larger valence-band offset.

ACKNOWLEDGMENTS

We are indebted to A. Ourmazd for critical reading and useful comments. We would like to thank H. Rücker for performing calculations of the potential barriers. The help of U. Penner in numerical calculation of the interface roughness scattering is acknowledged. The photoluminescence measurements were performed by S. Nilsson. The help of K. Tittelbach-Helmrich in the automatization of the capacitance measurements is acknowledged. We would like to express our gratitude to R. Winkler for technical assistance. We are indebted to H. Schneider for the preparation of the WTi-Schottky diodes. We acknowledge the support of the Volkswagen-Stiftung. I.N.Y. thanks the International Science Foundation for financial support.

[1] *Heterojunction Band Discontinuities: Physics and Device Applications*, edited by F. Capasso and G. Margaritondo (Elsevier, Amsterdam, 1987).

[2] D. V. Lang, in *Heterojunction Band Discontinuities: Physics and Device Applications* (Ref. 1), p. 377.

[3] N. Debbar, Dipankar Biswas, and Pallab Bhattcharya, Phys. Rev. B **10**, 1058 (1989).

[4] K. L. Jiao and W. Anderson, J. Appl. Phys. **73**, 271 (1993).

[5] G. Grumt and R. Pickenhain, Solid State Commun. **73**, 257 (1990).

[6] X. Letartre, D. Stievenard, and E. Barbier, Appl. Phys. Lett. **58**, 1047 (1991).

[7] L. Vescan, R. Apetz, and H. Lüth, J. Appl. Phys. **73**, 7427 (1993).

[8] K. Schmalz, I. N. Yassievich, H. Rücker, H. G. Grimmeiss, H. Frankenfeld, W. Mehr, H. J. Osten, P. Schley, and H. P. Zeindl, Phys. Rev. B **50**, 14 287 (1994).

[9] K. Schmalz, H. Rücker, H. P. Zeindl, and I. N. Yassievich, Superlattices Microstruct. **16**, 105 (1994).

[10] O. Chretien, R. Apetz, L. Vescan, A. Souifi, H. Lüth, K. Schmalz, and J. J. Koulmann, J. Appl. Phys. **78**, 5439 (1995).

[11] Qinhua Wang, Fang Lu, Dawei Gong, Xiangjung Chen, Jianbao Wang, Henghui Sun, and Xun Wang, Phys. Rev. B **50**, 18 226 (1994).

[12] X. Letartre, D. Stievenard, and E. Barbier, J. Appl. Phys. **69**, 7912 (1991).

[13] K. Kreher, Phys. Status Solidi A **135**, 597 (1993).

[14] K. Nauka, T. I. Kamins, J. E. Turner, C. A. King, J. L. Hoyt, and J. F. Gibbons, Appl. Phys. Lett. **60**, 195 (1992).

[15] I. N. Yassievich, K. Schmalz, and M. Beer, Semicond. Sci. Technol. **9**, 1763 (1994).

[16] M. M. Rieger and P. Vogel, Phys. Rev. B **48**, 14 276 (1993).

[17] X. Letartre, thesis, l'Université des Sciences et Techniques de Lille Flandres Artois, 1992.

[18] B. Laikhtman and R. A. Kiehl, Phys. Rev. B **47**, 10 515 (1993).

[19] A. Gold, Phys. Rev. B **35**, 723 (1987).

[20] A. Gold, Solid State Commun. **60**, 531 (1986).

[21] H. Sakaki, in *Physics of Nanostructures*, Scottish Universities Summer School in Physics, edited by J. H. Davies and A. R. Long (Institute of Physics, Bristol, 1992), p. 1.

[22] A. Gold, Phys. Rev. B **38**, 10 798 (1988).

[23] A. L. Efros, B. I. Shklovskii, in *Electron-Electron Interaction in Disordered Systems*, edited by A. L. Efros and M. Pollak (North-Holland, Amsterdam, 1985), p. 1.

[24] A. L. Efros and F. G. Pikus, Solid State Commun. **96**, 183 (1995).

[25] N. F. Mott, *Metal-Insulator Transitions* (Taylor & Francis, London, 1993).

[26] B. L. Shklovskii and A. L. Efros, *Electronic Processes in Doped Semiconductors* (Springer-Verlag, Berlin, 1984).

[27] I. S. Shlimak, A. L. Efros, and I. Ya. Yanchev, Fiz. Tekh. Poluprovodn. **2**, 262 (1977) [Sov. Phys. Semicond. **11**, 149 (1977)].